Constitutive theory for Recycled Aggregate Concretes subjected to high temperature

CrossMark

Guillermo Etse [a,b], Sonia M. Vrech [a,*], Marianela Ripani [b]

[a] CONICET, National Scientific and Technical Research Council, Center for Numerical and Computational Methods in Engineering, National University of Tucuman, Argentina
[b] CONICET – Materials and Structures Laboratory, University of Buenos Aires, Argentina

HIGHLIGHTS

- A thermodynamically consistent gradient poroplastic model is proposed.
- The RAC effect is considered by a concrete mixture recycling factor.
- Numerical results demonstrate good accuracy to predict failure behavior.

ARTICLE INFO

ABSTRACT

The use of recycled aggregates in concrete to partially substitute the natural ones has strongly increased in the last decades. Due to both, environmental and economical reasons, a relevant and increasing proportion of the concrete production in the developed countries is currently based on combinations between recycled and natural aggregates. As a result, a more eco-friendly constructive material is obtained which has gained significant impact in the construction market. Consequently, there is a need for accurate constitutive theories for predicting the mechanical behavior of Recycled Aggregate Concretes (RAC) subjected to severe loading conditions such as high temperature. In this work, a non-local gradient poroplastic material model is formulated for RAC composed by arbitrary proportions of recycled aggregates, when they are affected by long term exposures to high temperature. The model takes into account through one single parameter, the so-called *concrete mixture recycling factor*, the influence of the recycled aggregates proportion on the temperature-dependent yield condition, the local hardening/softening laws and the volumetric non-associativity. The last one accounts for the particular behavior of the plastic volumetric strains of RAC. The proposed dissipative constitutive theory is fully consistent with the thermodynamic laws. The predictive capabilities of the proposed constitutive formulation have been tested against experimental results on RAC specimens considering variable amounts of recycled aggregates in both, tensile and compressive regimes. Finally, the influence of the recycled aggregate inclusion and of its participation proportion on the localization properties and on the fundamental failure indicators is evaluated.

© 2016 Elsevier Ltd. All rights reserved.

1. Introduction

Climate change and global warming represent important topics in the field of the so called *Climate Change Science*. Starting from 1992, several countries joined into an international cooperation through the United Nations Framework Convention on Climate Change (UNFCCC) group, to synergistically adopt actions to limit the global temperature increase and to mitigate the resulting climate change. One of the main objectives of the UNFCCC is to control Greenhouse Gas Concentrations (GGC) in the atmosphere to prevent dangerous interference with the climate system, see Bjornberg [1].

Nowadays, the construction sector is one of the industrial activities that more resources and energy consumes. Particularly, according to recent surveys, emissions of GGC due to the concrete industry correspond to about 10% of the total, and almost the half of this proportion is due to the cement production [2]. To enhance the sustainability of this sector, the design of integrated recycling processes aimed to reducing wastes and to produce new *eco-friendly* materials is of particular interest, see a.o. Proske et al. [3].

* Corresponding author.
  E-mail addresses: getse@herrera.unt.edu.ar (G. Etse), svrech@herrera.unt.edu.ar (S.M. Vrech), mripani@fi.uba.ar (M. Ripani).

As a matter of fact, the possible production of concrete with recycled constituents (not only aggregates, but also alternative binders and/or natural fibers) is a feasible solution to reduce the environmental impact of the construction industry. Recently, numerous researches have addressed the possible structural use of concrete buildings manufactured with recycled aggregates, see a.o. Breccolotti and Materazzi [4], Li [5]. Moreover, several national and international codes have contributed to improve the knowledge of the use of such concretes in building constructions, see a. o. RILEM-TC-121-DRG [6] and NTC-2008 [7]. On the other hand, in the last years numerous experimental tests aimed at investigating the physical, mechanical and durability proprieties of concrete incorporating recycled aggregates have been performed, a.o. by Kou and Poon [8] and Folino and Xargay [9]. These studies have demonstrated that some mechanical properties of RAC may be generally lower than those of Natural Aggregate Concrete (NAC), however they are still sufficient for structural uses in civil constructions.

In recent years, the performance of RAC subjected to long term exposure to high temperatures and fire has became a subject of increasing interest in the scientific community. Thereby, the attention is focused on the evaluation and prediction of the mechanical property degradations of this material and the main differences with those of NAC. For instance, studies on the compressive mechanical capabilities of RAC subjected to elevated temperatures have been made a.o. by Zega and Di Maio [10] and Guo et al. [11]. A full review of the state of the art of the subject has been done by Cree et al. [12]. In all cases, the experimental evidence shows that the degradation of the mechanical properties of RAC under increasing temperature (compressive strength, tensile strength and elasticity modulus) is considerably more important than those of NAC.

From the numerical point of view, some constitutive formulations have been proposed to predict the mechanical behavior of RAC based on empirical considerations and mainly related to the compressive stress–strain relationships, see a.o. Du et al. [13]. Another formulation based on microplane theory has been developed by Li et al. [14]. In fact, none of the recent proposals can accurately reproduce the entire spectrum of possible failure modes of RAC subjected to arbitrary temperatures and for arbitrary proportions of recycled aggregates.

In this work a thermodynamically consistent gradient poroplastic material model is proposed to predict the mechanical response of RAC subjected to long term exposures of elevated temperatures and for all possible stress path, considering variable amounts of recycled aggregates into the cementitious material. A reformulation of the so-called temperature-dependent Leon–Drucker–Prager (TD-LDP) model for NAC by Ripani et al. [15], based on non-local gradient and fracture energy-based concepts is proposed to account for the recycled aggregate content and of its effect on the pre-peak stiffness, maximum strength capacity and post-peak regime, as well as on the inelastic dilatancy, when subjected to coupled thermo-mechanical actions. To account for the thermal degradation, and following Coussy [16], frozen entropy is incorporated, which describes the thermo-mechanic softening behavior. An isotropic and local hardening formulation that turns non-local in the softening regime is also accounted. Particularly, the strength decohesion in post-peak regime is controlled by two independent mechanism: (i) micro o macrocracking process, described by a fracture energy-based plasticity formulation according to Willam et al. [17] and Etse and Willam [18]; and (ii) degradation of the continuum or material located in between cracks, formulated by means of the gradient-based non-local plasticity based on Vrech and Etse [19]. Two characteristic lengths are included, one related to the fracture energy released in the active cracks during coupled thermo-mechanical processes and the other related to the gradient-based formulation. To realistically reproduce the strong

dependence of concrete failure modes on the acting confining pressure, temperature and initial porosity, both characteristic lengths are defined in terms of these variables.

The effects of the recycled aggregates and of the eventual presence of fly ash in the overall mechanical response behavior of RAC is taken into account by means of the so-called concrete mixture recycling factor which is introduced in the re-formulation of the hardening and softening laws, the maximum strength criterion and the non-associativity.

Fundamentals of the RAC mechanical behavior under room and high temperatures are described in Section 2. Basic assumptions of the constitutive theory and its formulation are highlighted in Sections 3 and 4. Section 5 reports the extension of the general constitutive gradient and fracture-based theory to account for RAC, which is the key contribution of this paper. Analysis of the numerical predictions of the proposed model is included in Section 7. Thereby, comparisons of the performances of the localization indicators for RAC and NAC are also included to illustrate the fundamental differences between the mechanical degradations in these two materials due to the combined action of temperature and mechanical loading. Finally the concluding remarks are discussed in Section 8.

2. Mechanical behavior of RAC

Experimental results on RAC samples in the literature, composed by different proportions of recycled aggregates lead to the following main conclusions regarding the mechanical response behavior of RAC. Under room temperature conditions, the failure behavior of RAC samples in the uniaxial compression test shows four main differences compared with that of the NAC, as follows: (i) reduced stiffness; (ii) smaller maximum strength; (iii) smaller ductility in post-peak regime, or smaller fracture energy; (iv) higher lateral deformation. This follows from the results by Rahal [20], Casuccio et al. [21], Folino and Xargay [9] and Lima et al. [22]. The last reference concludes also that the partial substitution of the finest portion of aggregates with fly ash, may lead to important increments of the uniaxial compressive strength of RAC, turning it similar to that of NAC. However, and due to the delayed binding action provided by the fly ash, the higher the content of this addition, the longer the time needed to achieve the maximum strength. Regarding the deformation capabilities of RAC, particularly the experimental campaign by Folino and Xargay [9] demonstrates that it considerably increases with the level of recycled concrete addition and this effect starts already in pre-peak regime. The inelastic volumetric expansion after peak reaches similar val-
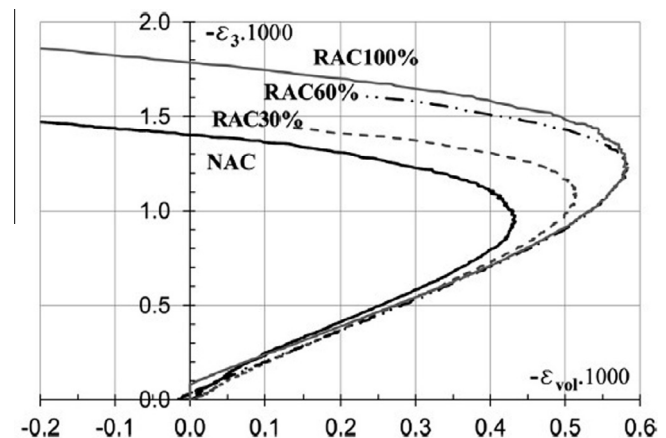

Fig. 1. Uniaxial compression: axial stresses vs. volumetric strain obtained from Folino and Xargay [9].

ues to those corresponding to NAC but under lower axial stresses, as can be observed in Fig. 1. Thus, it can be concluded that the inelastic lateral expansion in post-peak regime of RAC is more important than that of NAC and this difference increases with the amount of recycled aggregate. Particular material properties corresponding to the experimental campaign by Folino and Xargay [9] are shown in the third column of Table 2.

Under triaxial compression and room temperature condition, the sensitivity to the lateral confinement increases with the proportion of recycled aggregates due to the porosity increase. The last is, in turn, a consequence of the reduced workability of RAC in comparison to NAC. The higher sensitivity of RAC to the confinement pressure would mean that its apparent friction in the medium and high confinement regimes is higher than that of NAC, and it increases with the proportion of recycled aggregates. In the uniaxial tensile test, similarly to the compression case, a progressive strength reduction can be observed by increasing the percentage of recycled aggregates in the mix. Also a reduction of the fracture energy is obtained with increasing percentage of recycled aggregates, see a.o. Lima et al. [22], Silva et al. [23]. As in case of the uniaxial compressive strength, the RAC uniaxial tensile one increases when the finest portion of aggregates is substituted with fly ash. Regarding the temperature effect in the mechanical features of RAC and its comparison with NAC, the following could be concluded, based on the available results in the literature. In general, the effects of high temperature produce in RAC similar effects as in NAC, i.e. loss of stiffness, strength and fracture energy. It is generally accepted that the degradation of concrete mechanical features, particularly its maximum strength, when subjected to high temperature is mainly due to two factors: (i) the increase of vapor pressure arising from the evaporation of moisture; (ii) the initiation and development of crack caused by thermal stresses due to the temperature difference between different sectors of the involved concrete volume. However, as the moisture contents and the constitutive materials of aggregates and of their interfaces are quite different in RAC and NAC, the real effects of these two factors still require further understanding and investigations. So, although the overall effects of high temperature in NAC and RAC are quite similar, there are particular and relevant differences regarding the level of degradation caused by temperature. In this regard, while some authors like Chen et al. [24] conclude that under temperatures over 500 °C the compressive strength of RAC deteriorates more significantly than that of NAC, others like Kou et al. [25] conclude the opposite.

In the following sections a thermodynamically consistent non-local gradient poroplastic constitutive theory for concrete under high temperature is extended to account for the presence of recycled aggregates and fly ash in the concrete mixture. Then, the capabilities of the proposed model is evaluated by comparing its predictions with experimental results of uniaxial tensile and uniaxial/triaxial compression tests on RAC samples under room temperature, firstly, and after long term exposure to high temperature, secondly.

3. Thermodynamic framework of gradient poroplastic constitutive theory under non-isothermal conditions

The dissipative constitutive theory in this work is based on the mechanics of porous media that assumes the existence of a deformable skeleton and pore spaces with fluids, which are superimposed in time and space. The porosity of a given volume is the ratio between the fluid volume and the total volume. Permanent strains not only take place in the skeleton, but also in the fluid mass content due to the porosity variation either by mechanical or chemical effects.

Following the thermodynamically consistent gradient material theory for small strain kinematics by Svedberg and Runesson [26] and its extensions for poroplastic materials under non-isothermal conditions by Ripani et al. [15], the free energy density of the solid skeleton can be additively decomposed into three components, elastic, *local* and *non-local* plastic, as follows

$$\psi_s(\boldsymbol{\varepsilon}^e, n^e, \theta, \kappa_\xi, \nabla\kappa_\xi) = \psi^e(\boldsymbol{\varepsilon}^e, n^e, \theta) + \psi^l(\kappa_\xi, \theta) + \psi^{nl}(\nabla\kappa_\xi) \quad (1)$$

being $\boldsymbol{\varepsilon}^e$ the elastic strain tensor, n^e the elastic fluid mass content, θ the relative temperature ($\theta = T - T_0$ with T and T_0 the current and initial temperature usually adopted as 20, respectively), κ_ξ the internal variable with $\xi = p, s$ corresponding to the porous and solid phase respectively. A fundamental assumption in this gradient poroplastic theory is that the non-local effects are considered to be restricted to the state hardening/softening variable κ_ξ by means of $\nabla\kappa_\xi$.

The constitutive equations are obtained from Coleman's relations as

$$\boldsymbol{\sigma} = \rho \frac{\partial\psi_s}{\partial\boldsymbol{\varepsilon}^e}, \quad p = \rho \, \rho_f \frac{\partial\psi_s}{\partial n^e}, \quad s_s = \frac{\partial\psi_s}{\partial\theta} \quad (2)$$

being $\boldsymbol{\sigma}$ the stress tensor, p the pore pressure, s_s the specific entropy related to the solid skeleton, ρ and ρ_f the total and fluid phase densities respectively; while the local and non-local dissipative stresses are computed as

$$K_\xi^l = -\rho \frac{\partial\psi_s}{\partial\kappa_\xi}, \quad K_\xi^{nl} = \theta\nabla \cdot \left(\frac{\rho}{\theta} \frac{\partial\psi_s}{\partial\nabla\kappa_\xi} \right). \quad (3)$$

Considering the definition in Ripani et al. [15] of the free energy components ψ^e, ψ^l and ψ^{nl}, explicit solutions of the constitutive equations in Eq. (2) and of the dissipative stresses in Eq. (3) can be obtained.

In the realm of the flow theory of plasticity, the rates of plastic strain tensor, plastic mass and internal variables are defined as

$$\dot{\boldsymbol{\varepsilon}}^p = \dot\lambda \frac{\partial Q}{\partial\boldsymbol{\sigma}}, \quad \dot{m}^p = \dot\lambda \frac{\partial Q}{\partial p}, \quad \dot\kappa_\xi = \dot\lambda \frac{\partial Q}{\partial K_\xi} \quad (4)$$

where Q is the dissipative potential, $\dot\lambda$ the rate of the plastic multiplier and the total dissipative stress $K_\xi = K_\xi^l + K_\xi^{nl}$. To complete this formulation, the Kuhn–Tucker conditions are introduced

$$\dot\lambda \geqslant 0, \quad F(\boldsymbol{\sigma}, p, \theta, K_\xi) \leqslant 0, \quad \dot\lambda F(\boldsymbol{\sigma}, p, \theta, K_\xi) = 0 \quad (5)$$

where F symbolizes the yield function.

4. Temperature-dependent Leon–Drucker Prager model for NAC

In this section the gradient and fracture energy-based temperature-dependent Leon–Drucker–Prager model (TD-LDP) for NAC proposed by Ripani et al. [15] is summarized. This constitutive formulation follows the original thermodynamically consistent gradient-regularized material theory for small strain kinematics by Svedberg and Runesson [26], extended by Ripani et al. [15] for arbitrary thermodynamic states of open gradient poroplastic materials under non-isothermal conditions. Thereby, it is assumed that the plastic behavior is limited to the solid phase. Thus, in what follows the subindex ξ will not be used as only the solid phase is involved in the dissipation and non-linear response. Moreover, and as indicated before, non-local effects are only restricted to the scalar state variable.

The maximum strength surface of the TD-LDP model is obtained by combining the compressive meridian of the failure criterion by Leon [27] with the Drucker–Prager circular deviatoric shape. The mathematical description of the TD-LDP criterion for concrete in the space of the effective stresses is

$$F(^*\tau, ^*\sigma', \theta) = \frac{3}{2} \zeta(\theta) ^*\tau^2 + m_0 \beta(\theta) \left(\frac{^*\tau}{\sqrt{6}} + ^*\sigma' \right) - c_0 = 0 \quad (6)$$

with the effective first and second Haigh–Westergaard coordinates normalized respect to the uniaxial compressive strength

$$\sigma' = \frac{I_1}{3} - p, \quad \tau = \sqrt{2J_2} \quad \rightarrow \quad ^*\sigma' = \frac{\sigma'}{f_c}, \quad ^*\tau = \frac{\tau}{f_c} \quad (7)$$

being I_1 the first invariant of the stress tensor $\boldsymbol{\sigma}$, J_2 the second invariant of the deviatoric stress tensor $\boldsymbol{S}$, p the pore pressure and f_c the uniaxial compressive strength. Cohesive and frictional parameters, c_0 and m_0, are calibrated in terms of f_c and f_t, the uniaxial tensile strength, resulting

$$c_0 = 1, \quad m_0 = \frac{3}{2} \frac{\left(f_c^2 - f_t^2 \right)}{f_c f_t}. \quad (8)$$

The temperature-dependent functions $\zeta(\theta)$ and $\beta(\theta)$ are computed as

$$\zeta(\theta) = (1 - \gamma_1 \theta), \quad \beta(\theta) = \zeta(1 - \gamma_2 \theta), \quad (9)$$

being γ_1 and γ_2 the degradation parameters that must be calibrated from triaxial compression tests on concrete probes under different confining pressures and after long term exposure to low, medium and high temperature levels. Actually, the thermal depending factors ζ and β introduce in the constitutive equations the degradation due to temperature of the fundamental concrete mechanical properties, i.e. the cohesion and friction.

Beyond the elastic regime, the evolution of the yield surface in the hardening and softening regimes are encompassed by one single equation as follows

$$F(^*\tau, ^*\sigma', \theta, K^{p^+}, K^{p^-}) = \frac{3}{2} \zeta(\theta) ^*\tau^2 + m_0 \beta(\theta) K^{p^+} \left(\frac{^*\tau}{\sqrt{6}} + ^*\sigma' \right)$$
$$- K^{p^+} K^{p^-} = 0 \quad (10)$$

being K^{p^+} and K^{p^-} the pre- and post-peak dissipative stresses, varying according $K_0^{p^+} \leqslant K^{p^+} \leqslant 1$ and $1 \leqslant K^{p^-} \leqslant 0$. $K_0^{p^+} = 1$ represents the initial value of the hardening dissipative stress.

A non-associated plastic flow describes the inelastic behavior of concrete. The adopted plastic potential is based on a volumetric modification of the yield condition

$$Q(^*\tau, ^*\sigma', \theta, K^{p^+}, K^{p^-}) = \frac{3}{2} \zeta(\theta) ^*\tau^2 + m_0 \beta(\theta) \left(\frac{^*\tau}{\sqrt{6}} + \eta ^*\sigma' \right)$$
$$- K^{p^+} K^{p^-} = 0 \quad (11)$$

being η the volumetric non-associativity degree, which varies between $0 \leqslant \eta \leqslant 1$. The extreme case when $\eta = 0$ corresponds to the isochoric plastic flow while $\eta = 1$ results in associated plasticity.

5. The Extended TD-LDP for failure analysis of RAC

The well-established theoretical and mechanical TD-LDP framework has been extended to numerically reproduce the mechanical response and failure behavior of RAC after exposure to elevated temperatures under general load states.

In the following and separately, the modifications in the yield condition, maximum strength criterion, post-peak regime and the description of the inelastic volumetric deformation due to the considered amount of recycled aggregates are described.

5.1. Maximum strength surface and yield condition

The maximum strength criterion of the Extended TD-LDP follows from Eq. (6) as

$$F(^*\tau, ^*\sigma', \theta, \alpha_{RAC}) = \frac{3}{2} \zeta(\theta) ^*\tau^2 + m_{RAC} \beta(\theta) \left(\frac{^*\tau}{\sqrt{6}} + ^*\sigma' \right) - c_{RAC} = 0 \quad (12)$$

being the cohesive and frictional parameters for RAC

$$c_{RAC} = c_0 \alpha_{RAC}^2, \quad m_{RAC} = m_0 \alpha_{RAC} \quad (13)$$

and the so-called *concrete mixture recycling factor*

$$\alpha_{RAC} = 1 - \alpha_{r1} RA^{\alpha_{r2}} = \frac{f_c^{RAC}}{f_c} \quad (14)$$

which accounts for the degradation of the uniaxial compression strength of concrete due to the addition of recycled aggregates. Thereby RA is the content of recycled aggregate, while α_{r1}, α_{r2} are internal parameters to be calibrated from a set of uniaxial compression tests on concrete cylinders elaborated with a wide spectrum of different recycled aggregate contents. Fig. 2 shows the variation of the maximum strength surface of the Extended TD-LDP model with the aggregate content RA. In this case, the internal parameters $\alpha_{r1} = 0.00075$, $\alpha_{r2} = 1.25$ were adopted based on the set of experimental results by Folino and Xargay [9]. The material properties and adopted internal parameters are listed in the third column of Table 2 as well as in Table 1. In the same form to the maximum strength criterion, the expression of the yield condition in hardening/softening regime of the Extended TD-LDP model is modified from its original formulation in Eq. (10) to the following

$$F(^*\tau, ^*\sigma', \theta, \alpha_{RAC}, K_{RAC}^{p^+}, K_{RAC}^{p^-}) = \frac{3}{2} \zeta(\theta) ^*\tau^2 + m_{RAC} \beta(\theta) K_{RAC}^{p^+} \left(\frac{^*\tau}{\sqrt{6}} + ^*\sigma' \right)$$
$$- c_{RAC} K_{RAC}^{p^+} K_{RAC}^{p^-} = 0 \quad (15)$$

5.2. Ductility in pre-peak regime

RAC is characterized by a reduced ductility in pre- and post-peak regimes. Actually, the degradation of stiffness in RAC as compared to NAC is much quicker than that of peak strength. This effects even increases with the temperature. Different experimental results, see a.o. Li et al. [28] indicate that the reduced ductility of RAC is mainly due to the poorer mechanical properties of the Interfacial Transition Zone (ITZ) which is an important phase influencing the overall material response. The reduction of ductility in the pre-peak regime of RAC is taken into account in the Extended
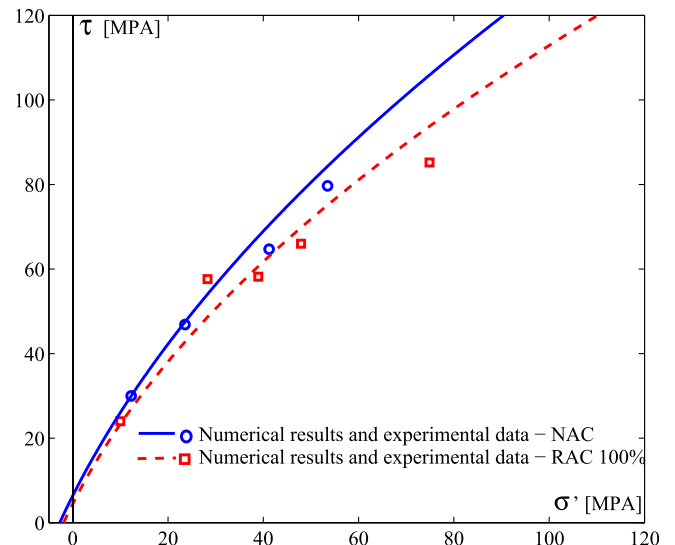
Fig. 2. Comparison of the TP-LDP model extended to RAC against experimental data in compressive regime at room temperature by Folino and Xargay [9].

Table 1
Common model internal parameters considered in the numerical analyses.

Hardening law – A_h; B_h; C_h	0.002; −0.13 MPa^{-1}; 0.00063 °C^{-1}
Local softening law – A_f	−2.20 °C^{-1}
Gradient softening law – A_g; B_g; C_g; D_g	0.2 mm^{-1}; 0.50; 0.000007 °C^{-1}; 0.00028 °C^{-1}
Maximum crack opening in Mode I – u_r	0.127 mm
Maximum gradient characteristic length – l_{cm}	70.00 mm
Maximum aggregate size – l_{ca}	18.00 mm
Gradient softening parameter – H^g	1.00 mm^{-1}
Minimum non-associative degree – η_0	0.12

TD-LDP model through the redefinition of the hardening ductility parameter. According Ripani et al. [15], the hardening dissipative stresses are given by

$$K_{RAC}^{p^+} = 0.1 + 0.9 \, \sin\left(\frac{\pi}{2} \frac{\|\varepsilon_h\|}{x_{RAC}}\right) \tag{16}$$

being ε_h the equivalent plastic strain in hardening and x_{RAC} the hardening ductility measure which, in this work, is defined not only as a function of the normalized confining pressure and the acting temperature, but also of the concrete mixture recycling factor as

$$x_{RAC} = \alpha_{RAC} A_h \exp\left(B_h \, ^*\sigma' + C_h \, \theta\right). \tag{17}$$

The coefficients A_h, B_h and C_h must be calibrated by triaxial compression tests under low and high confinement at room and high temperatures.

The variation of the hardening dissipative stresses $K_{RAC}^{p^+}$ in terms of the evolution of the hardening work $\frac{\|\varepsilon_h\|}{x_{RAC}}$ is well represented by means of the sinusoidal law chosen in Eq. (16). This law allows describing the typical hardening behavior observed in stress–strain-curves of normal concrete and RAC. In turn, Eq. (17) represents the exponential dependence of the pre-peak ductility on the confinement and temperature levels observed in experimental tests.

The evolution of the hardening dissipative stresses with variable confinement levels, temperatures and RAC content is shown in Fig. 3. As can be observed in this figure, concrete ductility during the evolution of the hardening dissipative stresses in pre-peak regime decreases with the amount of RAC in the concrete mixture, while increases with the applied confinement and temperature.
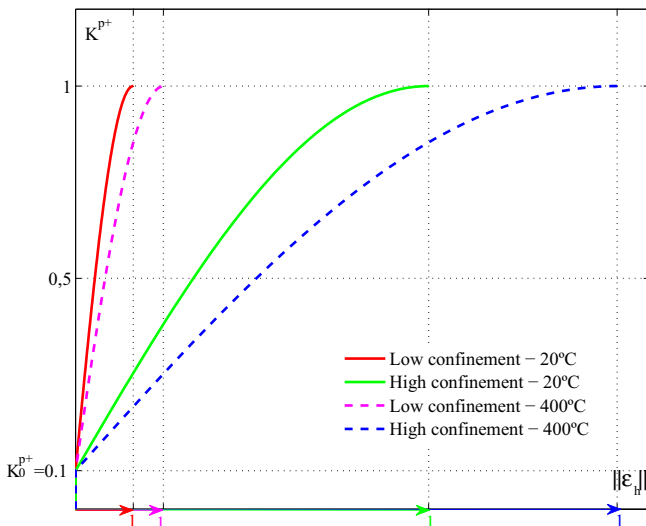

Fig. 3. Scheme of the evolution of the hardening dissipative stresses at variable confinement levels and temperatures.

5.3. Ductility in post-peak regime

Concrete failure process in post-peak regime of the TD-LDP model is define in terms of two mechanisms in parallel: one of them is based on fracture energy while the other one consists on a non-local gradient formulation. Thus, $K_{RAC}^{p^-}$ can be decomposed as

$$K_{RAC}^{p^-} = {}^f K_{RAC}^{p^-} + {}^g K^{p^-} \tag{18}$$

being ${}^f K_{RAC}^{p^-}$ the fracture energy-based strength decay associated to further propagations of active cracks, and ${}^g K^{p^-}$ the gradient-based softening mechanism account for the strength reduction due to the material degradation in-between active cracks. In the TD-LDP model formulation, both characteristic lengths, the fracture energy and the gradient one, are defined in terms of the confining pressure and the acting temperature, see Ripani et al. [15]. In this extension of the model formulation it is considered that the presence of recycled aggregates only affects the fracture energy-based strength degradation ${}^f K_{RAC}^{p^-}$. This is because, the fracture energy is directly related to the mechanical properties of both the aggregates and the ITZ. On the other hand, it is considered that the post-peak strength contribution related to the gradient based formulation, is not affected by the presence of recycled aggregates as this one is mainly related to the mechanical and thermal effects. The local or fracture-energy based dissipative stress is now defined as

$$^f K_{RAC}^{p^-} = \exp\left(-5 \frac{h_f^\theta}{u_{RAC}} \|\langle \varepsilon_f \rangle\|\right) \tag{19}$$

being ε_f the local fracture strain. The McAuley brackets indicate that only the tensile principal plastic strains contribute to the energy density during the fracture process. Then, u_{RAC} represents the maximum crack opening displacement of RAC in pure mode I of failure which is defined in terms of the concrete mixture recycling factor

$$u_{RAC} = \alpha_{RAC} u_r \tag{20}$$

with u_r the maximum crack opening displacement of the associated NAC, which is obtained when $\alpha_{RAC} \to 1$. The characteristic length h_f^θ represents the distance between active microcracks. It decreases under increasing confinement. Moreover, based on the experimental results by Chen et al. [24], It can be concluded that h_f^θ also depends on the acting temperature. More precisely, it decreases with increasing temperature, regardless the content of recycled aggregates. The dependence of h_f^θ on the confining pressure and the temperature is defined in the model as

$$h_f^\theta(^*\sigma', \theta) = \frac{h_t^\theta}{R_f(^*\sigma')} \qquad \text{with} \quad h_t^\theta = h_t \exp\left(A_f \theta\right) \tag{21}$$

Thereby, h_t is the maximum possible value of h_f^θ corresponding to mode I type of fracture under room temperature, A_f is a constant to be calibrated from experimental data, and

$$R_f(^*\sigma') = \begin{cases} 1 & \text{if } ^*\sigma' \geqslant 0 \\ 50.75 + 49.75 \sin\left(2 \, ^*\sigma' - \frac{\pi}{2}\right) & \text{if } -1.5 > \, ^*\sigma' > 0, \\ 100 & \text{if } ^*\sigma' \geqslant -1.5. \end{cases} \tag{22}$$

The pressure-dependent function R_f accounts for the ratio between the fracture energies G_f^{II} and G_f^I, which is considered as a constant during each infinitesimal evolution of the cracking process. Physical evidence shows that failure distribution and microcracking are enhanced with the increase of the confining pressure. The distance between cracks tends to zero with confinement levels greater than $1, 5f_c$. In contrast, microcracks coalesce in macro-defects, or even in one single crack, with decreasing confining pressures. Eq. (22) aims reproducing this mechanical behavior, leading to higher values of R_f with increasing confinement levels and consequently a lower value of h_f^θ in Eq. (21). In other words, the higher R_f the lower h_f^θ, which means that the ductility improves under increasing confinement.

The non-local dissipative stress in softening is defined as

$$^gK^{p^-}(\nabla\lambda) = -l_c^2 H^g \nabla^2\lambda \tag{23}$$

being H^g the non-local gradient modulus and l_c the width of the shear band in which the degradation of the material located in between active cracks ideally occurs. This geometrical measure, the so-called gradient-based characteristic length is defined here in terms of the acting confinement and temperature, but independently of the recycled aggregate content, as

$$l_c(^*\sigma',\theta) = \begin{cases} 0 & \text{if } ^*\sigma' \geqslant 0 \\ A_g l_{cm}(1+D_g\theta)\left\{1+\sin\left[B_g {}^*\sigma'(1+C_g\theta)-\frac{\pi}{2}\right]\right\} & \text{if } -1.5 < {}^*\sigma' < 0, \\ l_{cm}(1+D_g\theta) & \text{if } ^*\sigma' \geqslant -1.5. \end{cases} \tag{24}$$

being l_{cm} the maximum possible value of l_c, while A_g, B_g, C_g and D_g are internal parameters to be calibrated from sets of triaxial compression tests on concrete cylinders subjected to different confinements and temperatures.

5.4. Inelastic volumetric deformation and plastic potential

As detailed in Section 2, in the low confinement regime, the inelastic lateral deformation of concrete significantly increases with the amount of recycled aggregate. This is also a consequence of the poorer mechanical properties of the ITZ.

In the flow rule of plasticity, the theoretical framework for the formulation of this Extended TD-LDP for temperature-dependent RAC, the inelastic volumetric deformation is controlled by the degree of volumetric non-associativity, i.e. the terms of the plastic potential depending on the effective first invariant of the stress tensor. In this model formulation, the plastic potential is defined as

$$Q(^*\tau, {}^*\sigma', \theta, \alpha_{RAC}, K^{p^-}, K^{p^+}) = \frac{3}{2}\zeta(\theta) {}^*\tau^2 + m_{RAC}\beta(\theta)\left(\frac{{}^*\tau}{\sqrt{6}} + \eta_{RAC} {}^*\sigma'\right)$$
$$- c_{RAC} K_{RAC}^{p^+} K_{RAC}^{p^-} = 0 \tag{25}$$

with the degree of volumetric non-associativity η_{RAC} formulated in terms of the concrete mixture recycling factor as

$$\eta = \eta_0 - (1-\eta_0)\exp\left[\alpha_{RAC}(^*\sigma' - {}^*\sigma'_0) - 1\right] \tag{26}$$

Thereby, η_0 is the minimum value of the degree of volumetric non-associativity which is obtained on the edge of the plastic potential, where it intersects the hydrostatic axis. At this stress state the normalized form of the effective first stress coordinate approaches its maximum value $^*\sigma' = {}^*\sigma'_0$.

6. Localized failure indicator

The fundamental differences in the mechanical behavior of NAC and RAC can be best analyzed by the performance of the localization indicator which involves the formation of weak discontinuities in the strain rates or rather velocity gradient fields. Assuming that

the deformed solid can be divided in two subdomains named as "+" and "−" by an internal boundary with normal N, and according to Maxwell's compatibility theorem by Truesdell and Toupin [29], this jump of the velocity gradient field is a rank one second order tensor which must satisfy

$$[[\nabla\dot{u}]] = \dot{\gamma}M \otimes N, \tag{27}$$

where M denotes the polarization vector and $\dot{\gamma}$ an scalar factor defining the magnitude of the jump. The situation described by Eq. (27) has its analogous counterpart in fracture mechanics, corresponding to a Mode I fracture for $M\|N$ and Mode II fracture for $M \perp N$. The strain rate discontinuity is then defined by the symmetrized dyadic of the unit vectors M and N, i.e.

$$[[\dot{\varepsilon}]] = [[\nabla^{sym}\dot{u}]] = \frac{1}{2}\dot{\gamma}(M \otimes N + N \otimes M) = \dot{\gamma}(M \otimes N)^{sym} \tag{28}$$

Balance of linear momentum across the discontinuity surface leads to the localization condition

$$t = N \cdot [[\dot{\sigma}]] = N \cdot E^{ep} : [[\dot{\varepsilon}]] = \dot{\gamma}N \cdot E^{ep} : (M \otimes N)^{sym} = \dot{\gamma}Q^{ep} \cdot M \dot{=} 0 \tag{29}$$

where the elastoplastic localization (acoustic) tensor is defined as $Q^{ep} = N \cdot E^{ep} \cdot N$, being E^{ep} the tangential elastoplastic material operator. According to Eq. (29), discontinuous bifurcation initiates when the localization tensor exhibits a singularity, i.e. $\det(Q^{ep}) = 0$, for some directions M and N.

In gradient poroplasticity, as the case of the constitutive theory for RAC in this paper, the gradient elastoplastic localization tensor for drained condition can be written as Vrech and Etse [30] and Mroginski and Etse [31]

$$Q_s^{epg} = Q_s^e - \frac{1}{h+h^g}a^m \otimes a^n \tag{30}$$

with the elastic localization tensor $Q_s^e = N \cdot E_s^e \cdot N$, being E_s^e the elastic tensor and

$$a^m = \frac{\partial Q}{\partial\sigma'} : E_s^e \cdot N \tag{31}$$

$$a^n = \frac{\partial F}{\partial\sigma'} : E_s^e \cdot N \tag{32}$$

$$h = \frac{\partial F}{\partial\sigma'} : E_s^e : \frac{\partial Q}{\partial\sigma'} + H\frac{\partial F}{\partial K_s}\frac{\partial Q}{\partial K_s} \tag{33}$$

$$h^g = H^g\frac{\partial F}{\partial K_s}\frac{\partial Q}{\partial K_s}\left(\frac{2\pi l_c}{\delta}\right)^2 \tag{34}$$

Moreover, δ is the final localization or wave length, H and H^g are the thermodynamically consistent local and non-local hardening/-softening modulus.

In the above equations, the subindex s means that the indicated tensor corresponds to the solid portion of the porous media. It should be reminded that all material operators belong only to the solid portion.

7. Numerical analysis

In this section, the predictive capabilities of the proposed material model to reproduce the failure behavior of RAC are verified at room temperature and after exposure to elevate temperatures. Variable content of recycled aggregates and stress paths are considered in the analyses.

At the finite element (FE) level, the dual-mixed FE formulation proposed by Svedberg and Runesson [26] is considered for the numerical analyses. Fig. 4 shows the adopted FE discretization based on constant strain triangles (CST), and the boundary conditions. The last, correspond to inhomogeneous distributions of the

stress and strain fields. In Fig. 5 the flowchart of the numerical implementation of the proposed microplane model is summarized.

As it is well known, and due to its intrinsic locking, CST finite elements lead overestimations of the failure distribution when considered in the framework of non-linear material behavior simulations. To bypass this shortcoming, sufficiently fine FE discretizations shall be considered. When doing so, the CST finite elements offer two relevant advantages. On the one hand, they are associated to very stable numerical solutions in pre and post-peak regimes. This allows reproducing highly non-linear deformation histories without being affected by spurious bifurcation conditions. On the other hand, they are numerically very efficient from the time-consuming stand point due to high convergence rate of the dual mixed method originally proposed by Svedberg and Runesson [26] for the evaluation of both $\Delta\lambda$ and $\nabla^2(\Delta\lambda)$ in the framework of CST finite element formulations. In case of gradient plasticity a fundamental consideration to assure that the FE discretization with CST is sufficiently reach is that at least two finite elements are included in the shear band. This was verified in these numerical analyses and in the considered FE discretizations.

In the numerical analyses in this section, under room temperature conditions, three types of stress paths were considered with different content of recycled aggregates: uniaxial tensile test, uniaxial compression test and triaxial compression test. Due to the limited experimental data published in the literature, only the stress path of the uniaxial compression test is considered in the analysis of model predictive capabilities for the case of RAC failure behavior under high temperature. The particular geometry of the rectangular FE patch in Fig. 4, and its stress condition (axisymmetric or plane stress) were varied in the different numerical analyses attending the experimental boundary conditions.

In all considered stress histories, incremental axial loads are applied under displacement control on the nodes along the specimen top while the lateral confinement is applied under force control on the nodes along the external side of the FE mesh. Common and particular model internal parameters and material properties adopted in the numerical analyses are summarized in Tables 1 and 2. Thereby are included all parameters of the hardening and softening (local and non-local) laws.
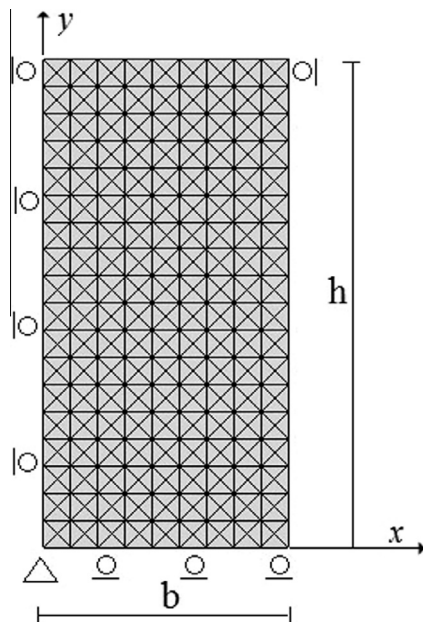

Fig. 4. FE discretization and inhomogeneous boundary conditions of a quarter of a concrete specimen (cylindrical or rectangular panel) considered in the numerical analyses.
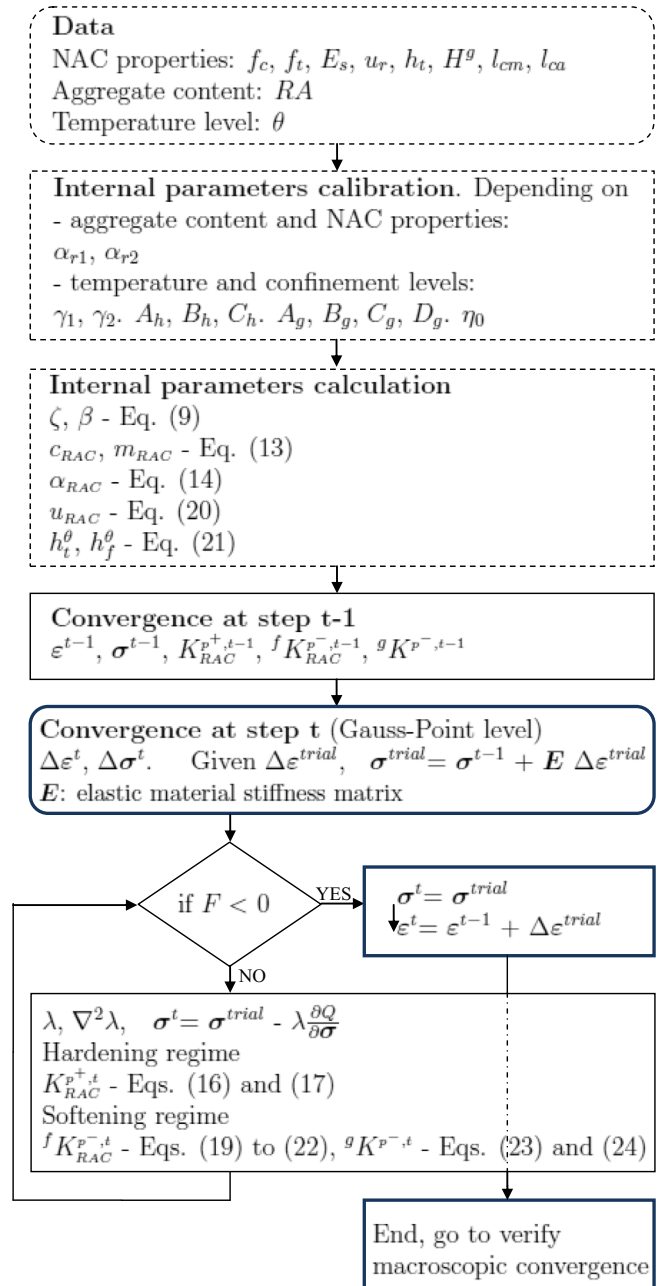

Fig. 5. Flowchart of local Newtons method used for step-by-step integration of the FE method.

7.1. Analysis at room temperature

Firstly, the numerical predictions of the uniaxial experimental tests by Akita et al. [32] performed under room temperature on concrete prisms of $100 \times 100 \times 400$ mm are considered. In this case, two FE patches like the one indicated in Fig. 4 were adopted, one of top of the other, to reproduce the 1×4 relation between specimen width and high, while plane stress conditions were considered. Moreover, the material strength of the 4 CST finite elements corresponding to the square on the extreme right hand side of the bottom row in the FE array was reduced in 10% to represent the notched considered in the experimental tests by Akita et al. [32].

Fig. 6 shows the prediction of the proposed model to the uniaxial tensile tests for NAC and RAC with 100% recycled aggregate con-

Table 2
Particular material properties and model internal parameters considered in the numerical analyses.

	Akita et al. [32]	Guo et al. [11]	Folino and Xargay [9]	Chen et al. [24]	Leeet al. [33]	Hurlbut [34]
f_c – [MPa]	22.5	56.52	36.52	39.57	21	22
f_t – [MPa]	2.5	6.28	4.04	4.4	2	2.2
E_s – [GPa]	11.0	34.91	31.67	23.8	11.0	19.3
α_{r1}	0.00055	0.000375	0.00075	0.00015	–	–
α_{r2}	1.05	1.2	1.25	1.02	–	–
γ_1 – [°C^{-1}]	0	0	0	0.00130	0.00126	0.00126
γ_2 – [°C^{-1}]	0	0	0	0.00042	0.0056	0.0056

tent. The comparison with the experimental results shows very good agreement regarding peak strength, post-peak behavior and residual strength, for both NAC and RAC cases.

In the following, model predictions of the uniaxial compressive behavior of RAC are evaluated. Thereby, the experimental results by Guo et al. [11] are considered for NAC and RAC with 100% content of recycled aggregates. Axisymmetric stress conditions are considered to model the concrete cylindrical probes of 150×300 mm dimensions, under non-homogeneous boundary conditions. The comparisons between experimental and numerical results in Fig. 7, demonstrate the predictive capabilities of the proposed model regarding pre- and post-peak behaviors, peak strength, and inelastic deformation of RAC in the uniaxial compression test.

Next, the uniaxial compression experimental results by Folino and Xargay [9] on concrete cylinders of 100×200 mm with different contents of recycled aggregates are considered. The comparison between numerical and experimental results in Fig. 8, for NAC and RAC with 30%, 60% and 100% recycled aggregate contents show good agreement regarding both the pre-peak behavior and the peak strength for all different cases. The post-peak behaviors obtained by Folino and Xargay [9] show no softening but very ductile responses. This is quite unusual in concrete uniaxial compression tests. Therefore, the accuracy of the numerical predictions in this regime cannot be evaluated.

Finally, the triaxial compression experimental results by Folino and Xargay [9] on concrete cylinders of 100×200 mm are considered. They were performed with different content of recycled

Fig. 7. Experimental results by Guo et al. [11] of uniaxial compression tests on cylinders composed by NAC and RAC (100% recycled aggregate content), and numerical predictions with proposed constitutive model.

Fig. 8. Experimental results of uniaxial compression tests with NAC and RAC with different contents of recycled aggregates by Folino and Xargay [9], and numerical predictions with the proposed constitutive model.

aggregates and different lateral confinements. Fig. 9 illustrates the comparison between experimental and numerical results for the RAC specimens with 60% of recycled aggregate content. Again, very good agreements between the numerical predictions with the proposed model and the experimental results for all different confinement pressures are obtained. It is very interesting to note that the model is able to reproduce the variation of ductility and peak strength of RAC with the applied confinement under triaxial stress conditions.

7.2. Analysis after exposure to elevated temperature

In this section the temperature-dependent failure behavior of NAC and RAC subjected to uniaxial and triaxial compression tests
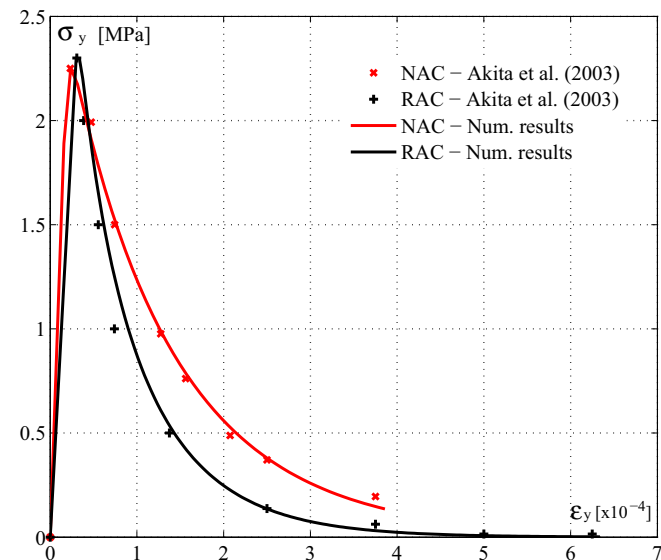

Fig. 6. Experimental results on uniaxial tensile test by Akita et al. [32] for NAC and RAC with 100% recycled aggregate, and numerical predictions with the proposed model.
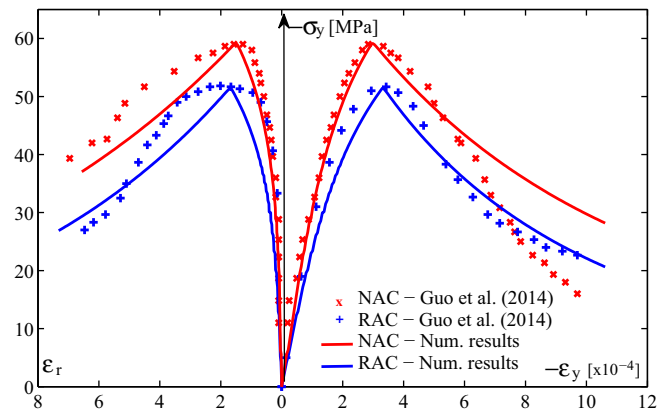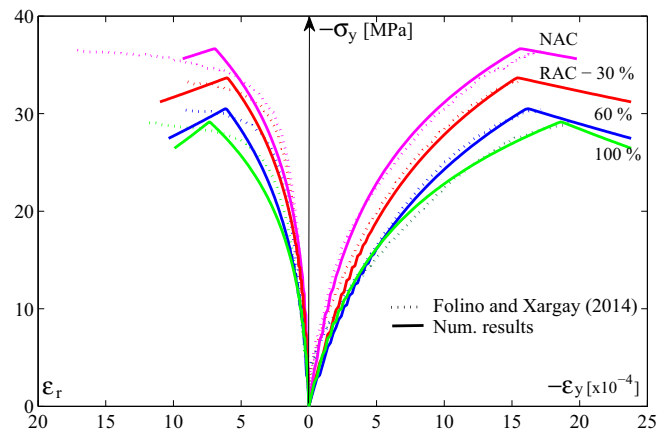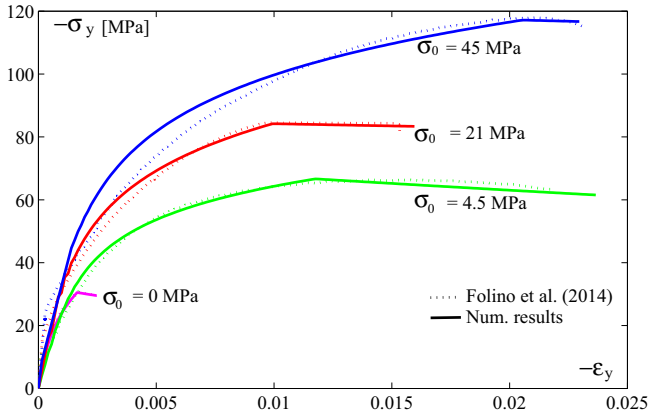
Fig. 9. Triaxial compression tests by Folino and Xargay [9] for RAC with 60% recycled aggregate content and numerical predictions with the proposed model.

Fig. 11. Experimental results by Hurlbut [34] and numerical predictions of triaxial compression tests on NAC specimens under room temperature conditions and after long term exposure to different temperatures.

are evaluated regarding the numerical predictions of the TD-LDP constitutive model. In Fig. 10 the model predictions of the uniaxial compression test in terms of axial stresses vs. axial strains are compared with the experimental results by Lee et al. [33] on NAC cylindrical specimens of 101.6 × 203.2 mm at room temperature and after long term exposure to high temperature. The numerical results agree very well with the experimental data for all different temperature levels (from 20 °C to 600 °C), concerning the loss of both, stiffness in pre-peak regime and peak strength with increasing temperature. Another effect that can be clearly recognized from the experimental and numerical results in Fig. 10 is the great increment of the ductility together with the peak strength reduction in both the pre- and post-peak regimes as the temperature increases.

It is very interesting to evaluate the effect of the lateral confinement in triaxial compression tests performed on NAC damaged by temperature. In Fig. 11 the results obtained by Hurlbut [34] for the triaxial compression tests on cylinder concretes of 108 × 216 mm at room temperature and different confinement levels are compared with the model predictions. In the same figure, the model predictions corresponding to 500 °C are evaluated. It can be concluded that the confinement pressure contributes to reduce not only the lateral dilatancy of concrete, but mainly the strength degradation caused by temperature.

Next, the proposed model predictions of failure behavior of RAC under different temperature conditions are evaluated. Unfortunately, very few available experimental results can be found in

the literature regarding failure behavior of RAC under medium and high temperature. Here the experimental results by Chen et al. [24] on RAC cylindrical specimens of 150 × 300 mm after long term exposure to different temperatures are considered.

Fig. 12 shows the comparison between the experimental results by Chen et al. [24] and the numerical predictions with the proposed model of uniaxial compression tests on RAC probes composed by 100% of recycled aggregates. These results show very good predictions in terms of pre-peak stiffness, peak strength, strain at peak stress, post-peak behavior and also of residual strength for all different temperatures, including the very high one. It should be noted that the model captures very accurately the strong reduction of stiffness and peak strength that takes place when the applied temperature in RAC specimens goes beyond the 200 °C and, moreover, beyond 400 °C.

It is also very interesting to compare in Fig. 13 the deformed meshes at residual stages of the uniaxial compression tests under room temperature and after exposure to 400 °C. It can be clearly observed the dramatic increase of both the deformability and shear band width of RAC when it is subjected to long term exposure to high temperature.

7.3. Localization analysis

In this section, the performance of the localization indicator of RAC for different content of recycled aggregates is evaluated. This indicator signalizes the onset of discontinuous bifurcation related to the strain rate field, under consideration of continuous hydraulic fields. As detailed in the previous sections, the strength decay in the post-peak regime of the proposed constitutive theory is described by means of both a non-local gradient based formulation and a fracture-energy based one. Being the non-local gradient characteristic length defined in terms of the acting temperature and confining pressure, its value may strongly reduce the very localized form of concrete failure in the tensile regime and also for same extreme temperature conditions. So, even Fig. 14 shows the performance of the normalized indicator for localized failure of the proposed constitutive model at peak strength of the uniaxial compression test for NAC and RAC with different contents of recycled aggregate by Folino and Xargay [9]. They are all normalized regarding the determinant of the elastic localization tensor of NAC.

The critical directions for localization signaled by the normal to the potential discontinuity surface for all analyzed cases are depicted in Table 3. Thereby are included not only the cases corresponding to the uniaxial compression test but also to the direct shear test.
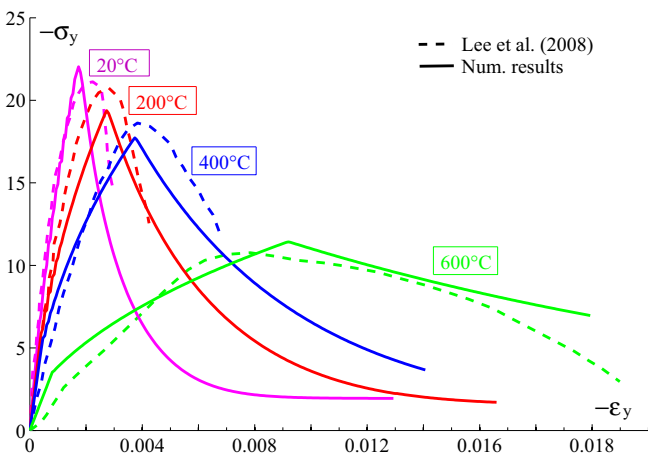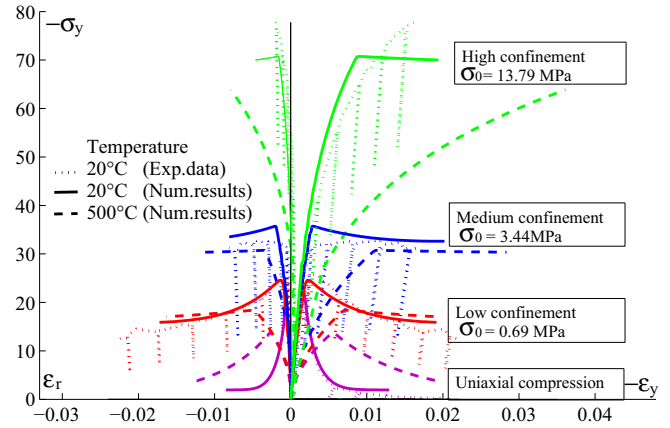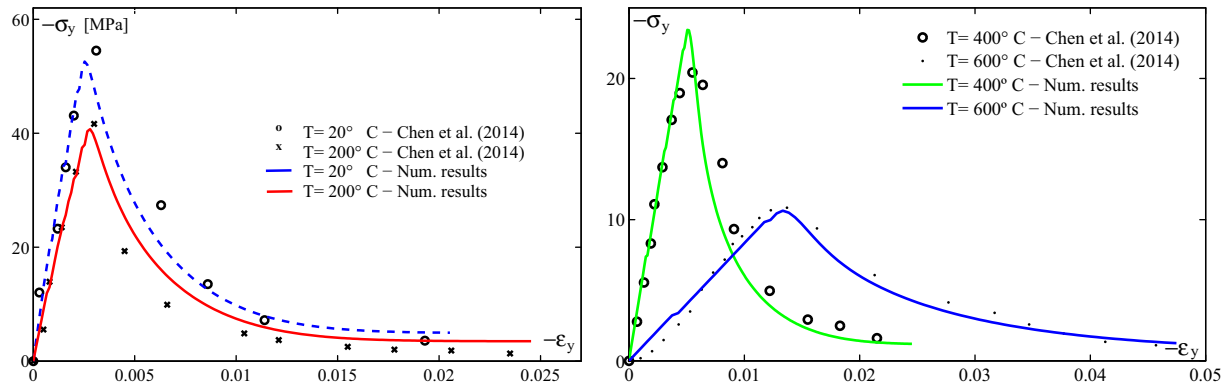

Fig. 10. Experimental results by Lee et al. [33] and numerical predictions of uniaxial compression tests on NAC specimens under room temperature conditions and after long term exposure to different temperatures.

Fig. 12. Experimental results by Chen et al. [24] and numerical predictions of uniaxial compression tests on RAC specimens with 100% aggregate content under room temperature conditions and after long term exposure to different temperatures.
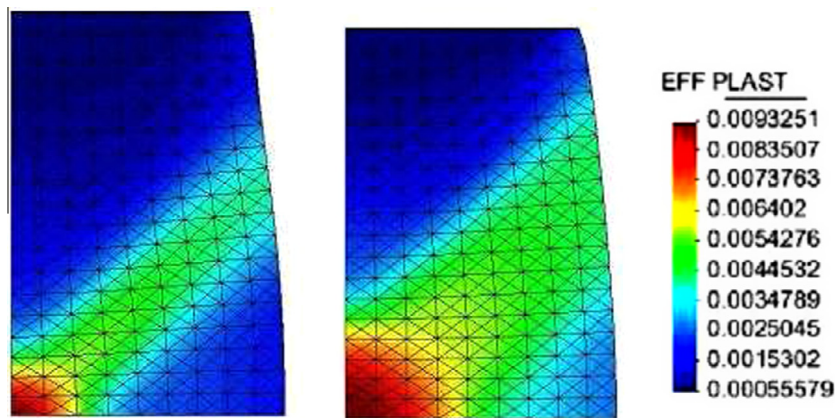

Fig. 13. Deformed pattern and equivalent plastic strain distribution at residual stage of the FE analyses corresponding to uniaxial compression test at room temperature and after exposure to 400 °C by Chen et al. [24].
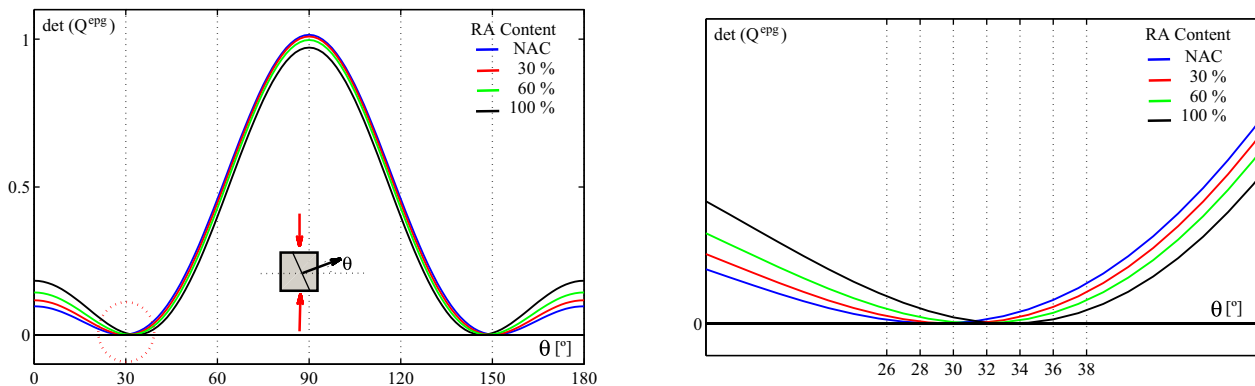

Fig. 14. Performance of the normalized localization indicator at peak stress of the uniaxial compression test on NAC and RAC specimens (with different contents of recycled aggregates).

From these results, three important conclusions arise. Firstly, increasing proportions of recycled aggregates lead to reductions of the maximum wave propagation velocities or stiffness at peak stress of the uniaxial compression test. Secondly, the indicator of localization tensor approaches zero but remains positive in all different cases, indicating that the involved differential equations do not turn ill defined. Finally, the direction of the potential discontinuity surface rotates towards the horizontal direction as the proportion

of recycled aggregate increases. In other words, the potential for compression splitting failure modes of RAC is lower than that of NAC.

In case of the peak strength of the direct shear test the same effect is obtained, i.e. the inclination of the potential discontinuity with respect to the horizontal axis reduces with increasing proportion of recycled aggregates. Also, the localization indicator remains positive for NAC and all RAC cases.

Table 3
Critical angles of the normal to the discontinuity surface in the peak stress of the uniaxial compression test and direct shear test, for RAC with different contents of recycled aggregate.

Content of recycled aggregates [%]	Critical localization angle [°]	
	Uniaxial compression test	Direct shear test
0	28.5	18
30	30	19.5
60	31.5	20.25
100	33	21

8. Conclusions

In this work, a thermodynamically consistent gradient-based poroplastic constitutive theory was extended to simulate the failure behavior under high temperature of RAC composed by arbitrary content of recycled aggregate. The main features of RAC as compared to NAC are taken into account by means of consistent reformulations of the maximum strength criterion, the hardening law and the fracture-energy based softening formulation of the model in terms of the so-called *concrete mixture recycling factor*. This parameter is also considered to reformulate the volumetric non-associative flow rule of the constitutive law to account for the larger plastic dilatancy of RAC in comparison to NAC.

The numerical results included in this work demonstrate the accuracy of the proposed model to predict failure behavior of RAC subjected to different stress histories and composed by different contents of recycled aggregates. Under both room temperature and high temperature conditions, the proposed model is able to capture the influence of the content of recycled aggregates on the failure response behavior. In this regard, the analysis of the localization indicator in terms of the determinant to the localization tensor demonstrates that at peak stress of the uniaxial compression test, the direction of the potential crack in case of RAC turns toward the normal direction to the applied load as the content of recycled aggregate increases.

Acknowledgment

References

[1] K. Bjornberg, Rational climate mitigation goals, Energy Policy 56 (2013) 285–292.

[2] National Ready Mixed Concrete Association, Concrete CO_2 Fact Sheet. Silver Spring, MD, <http://www.nrmca.org>, 13, 2012.

[3] T. Proske, S. Hainer, M. Rezvani, C. Graubner, Eco-friendly concretes with reduced water and cement contents – mix design principles and laboratory tests, Cem. Concr. Res. 51 (2013) 38–46.

[4] M. Breccolotti, A. Materazzi, Structural reliability of eccentrically-loaded sections in RC columns made of recycled aggregate concrete, Eng. Struct. 32 (11) (2010) 3704–3712.

[5] X. Li, Recycling and reuse of waste concrete in China: Part II. Structural behaviour of recycled aggregate concrete and engineering applications, Resour. Conserv. Recycl. 53 (3) (2009) 107–112.

[6] RILEM-TC-121-DRG, Specifications for concrete with recycled aggregates, Mater. Struct. 27 (1994).

[7] NTC-2008, Norme tecniche per le costruzioni (Italian Recommendations) 29 Decreto Ministeriale 14 gennaio, 2008.

[8] S. Kou, C. Poon, Enhancing the durability properties of concrete prepared with coarse recycled aggregate, Constr. Build. Mater. 35 (2012) 69–76.

[9] P. Folino, H. Xargay, Recycled aggregate concrete-mechanical behavior under uniaxial and triaxial compression, Constr. Build. Mater. 56 (2014) 21–31.

[10] C. Zega, A. Di Maio, Recycled concrete made with different natural coarse aggregates exposed to high temperature, Constr. Build. Mater. 23 (2009) 2047–2052.

[11] Y. Guo, J. Zhang, G. Chen, Z. Xie, Compressive behaviour of concrete structures incorporating recycled concrete aggregates, rubber crumb and reinforced with steel fibre, subjected to elevated temperatures, J. Cleaner Prod. 72 (2014) 193–203.

[12] D. Cree, M. Green, A. Noumowé, Residual strength of concrete containing recycled materials after exposure to fire: a review, Constr. Build. Mater. 45 (2013) 208–223.

[13] T. Du, W. Wang, Z. Liu, H. Lin, T. Guo, The complete stress–strain curve of recycled aggregate concrete under uniaxial compression loading, J. Wuhan Univ. Technol.-Mater. Sci. Ed. 25 (5) (2010) 862–865.

[14] J. Li, J. Xiao, J. Huang, Microplane model for recycled aggregate concrete. 2nd International Conference on Waste Engineering and Management – ICWEM 2010, 2010.

[15] M. Ripani, G. Etse, S. Vrech, J. Mroginski, Thermodynamic gradient-based poroplastic theory for concrete under high temperatures, Int. J. Plast. 61 (2014) 157–177.

[16] O. Coussy, Mechanics of Porous Continua, John Wiley & Sons, 1995.

[17] K. Willam, B. Hurbult, S. Sture, Experimental constitutive aspects of concrete failure, US–Japan Seminar on Finite Element Analysis of Reinforced Concrete Structures, ASCE-Special Publication, 1985.

[18] G. Etse, K. Willam, A fracture energy-based constitutive theory for inelastic behavior of plain concrete, J. Eng. Mech. ASCE 120 (1994) 1983–2011.

[19] S. Vrech, G. Etse, Gradient and fracture energy-based plasticity theory for quasi-brittle materials like concrete, Comput. Meth. Appl. Mech. Eng. 199 (1-4) (2009) 136–147.

[20] K. Rahal, Mechanical properties of concrete with recycled coarse aggregate, Build. Environ. 42 (1) (2007) 407–415.

[21] M. Casuccio, M. Torrijos, G. Giaccio, R. Zerbino, Failure mechanism of recycled aggregate concrete, Constr. Build. Mater. 22 (7) (2008) 1500–1506.

[22] C. Lima, A. Caggiano, C. Faella, E. Martinelli, M. Pepe, R. Realfonzo, Physical properties and mechanical behaviour of concrete made with recycled aggregates and fly ash, Constr. Build. Mater. 47 (2013) 547–559.

[23] R. Silva, J. de Brito, R. Dhir, Tensile strength behavior of recycled aggregate concrete, Constr. Build. Mater. 83 (2015) 108–118.

[24] G. Chen, Y. He, H. Yang, J. Chen, Y. Guo, Compressive behavior of steel fiber reinforced recycled aggregate concrete after exposure to elevated temperatures, Constr. Build. Mater. 71 (2014) 1–15.

[25] S. Kou, C. Poon, M. Etxeberria, Residue strength, water absorption and pore size distributions of recycled aggregate concrete after exposure to elevated temperatures, Cem. Concr. Compos. 53 (2014) 73–82.

[26] T. Svedberg, K. Runesson, A thermodynamically consistent theory of gradient-regularized plasticity coupled to damage, Int. J. Plast. 13 (6-7) (1997) 669–696.

[27] A. Leon, Ueber das Mass der Anstrenung bei Beton, Ing. Arch. 4 (1935) 421–431.

[28] W. Li, J. Xiao, Z. Sun, S. Kawashima, S. Shah, Interfacial transition zones in recycled aggregate concrete with different mixing approaches, Constr. Build. Mater. 35 (2012) 1045–1055.

[29] C. Truesdell, R. Toupin, The Classical Field Theories, Springer, 1960.

[30] S. Vrech, G. Etse, Geometrical localization analysis of gradient-dependent parabolic Drucker–Prager elastoplasticity, Int. J. Plast. 22 (5) (2006) 943–964.

[31] J. Mroginski, G. Etse, Discontinuous bifurcation analysis of thermodynamically consistent gradient poroplastic, Int. J. Solids Struct. 9 (1) (2014) 1834–1846.

[32] H. Akita, H. Koide, M. Ojima, Tensile behavior of a recycled concrete, V.C. Ki, I. H. Marshall, A.M. Brandt (Eds.), Proc. Inter. Symp. Britte Matrix Composites 7, Warsaw, 2003, 263–268.

[33] J. Lee, Y. Xi, K. Willam, Properties of concrete after high-temperature heating and cooling, ACI Mater. J. 105 (3) (2008) 334–341.

[34] B. Hurlbut, Experimental and computational investigation of strain-softening in concrete (Master thesis), University of Colorado, 1985.